

# Accelerating Neural Network Inference with Processing-in-DRAM: From the Edge to the Cloud

**Geraldo F. Oliveira**  
ETH Zürich

**Juan Gómez-Luna**  
ETH Zürich

**Saugata Ghose**  
University of Illinois Urbana-Champaign

**Amirali Boroumand**  
Google

**Onur Mutlu**  
ETH Zürich

**Abstract**—Neural networks (NNs) are growing in importance and complexity. A neural network’s performance (and energy efficiency) can be bound either by computation or memory resources. The processing-in-memory (PIM) paradigm, where computation is placed near or within memory arrays, is a viable solution to accelerate memory-bound NNs. However, PIM architectures vary in form, where different PIM approaches lead to different trade-offs. Our goal is to analyze, discuss, and contrast DRAM-based PIM architectures for NN performance and energy efficiency. To do so, we analyze three state-of-the-art PIM architectures: (1) UPMEM, which integrates processors and DRAM arrays into a single 2D chip; (2) Mensa, a 3D-stack-based PIM architecture tailored for edge devices; and (3) SIMDRAM, which uses the analog principles of DRAM to execute bit-serial operations. Our analysis reveals that PIM greatly benefits memory-bound NNs: (1) UPMEM provides  $23\times$  the performance of a high-end GPU when the GPU requires memory oversubscription for a general matrix–vector multiplication kernel; (2) Mensa improves energy efficiency and throughput by  $3.0\times$  and  $3.1\times$  over the Google Edge TPU for 24 Google edge NN models; and (3) SIMDRAM outperforms a CPU/GPU by  $16.7\times/1.4\times$  for three binary NNs. We conclude that the ideal PIM architecture for NN models depends on a model’s distinct attributes, due to the inherent architectural design choices.

## Introduction

■ Neural networks (NNs) [1–3] are becoming increasingly important for many daily activities, from routine tasks such as commute traffic estimation [4] to critical tasks such as medical diagnosis [5]. NN algorithms are rapidly evolving,

which has led to many different types of NN models [6–41]. Such NN algorithms behave as either *compute-bound* workloads (i.e., when computing resources are the main performance bottleneck) or as *memory-bound* workloads (i.e., when memory resources are the main performance bottleneck) depending on the NN model [42–51].

A common approach to improve the performance of compute-bound NNs is to design compute-centric accelerators [6, 42, 46, 48, 52–62], where a significant portion of hardware resources are dedicated to the processing elements of the accelerator. Compute-centric NN accelerators aim to speed up two main operations that many NN models rely on [44]: multiply-and-accumulate (MAC), largely used for convolutions; and matrix-vector multiplications (MVMs). Similarly, various approaches to improve the performance of memory-bound NNs have been proposed [45, 63–73]. One such approach is processing-in-memory (PIM) [74–85], where computation is (1) placed near 2D [69, 86–110] or 3D [45, 63, 64, 67, 111–166] memory arrays (processing-near-memory, PNM) or (2) performed using the memory arrays themselves (processing-using-memory, PUM) [65, 70–72, 135, 167–203].<sup>1</sup> PNM and PUM can be implemented using different memory technologies [75], including SRAM [71, 99, 107, 110, 177, 178], DRAM [45, 64, 87, 100, 111, 123, 125, 128, 131–135, 142, 143, 146, 152, 157, 193, 195, 196], and resistive RAM (ReRAM) [65, 70, 121, 174, 175, 183, 188, 189, 199, 200, 202]. Independent of the memory technology, PIM allows NNs to enjoy higher memory bandwidth, shorter memory access latency, and lower energy per bit [75].

Our *goal* is to analyze, discuss, and contrast the benefits and drawbacks of different PIM architectures for NN performance and energy efficiency in different computing environments (i.e., edge devices and cloud servers). In this work, we focus on DRAM-based PIM, and NN inference in three different DRAM-based PIM architectures: (1) UPMEM [88, 90–92, 204, 205], a large-scale 2D-based PNM architecture, which integrates several simple general-purpose processing cores near DRAM arrays (inside a DRAM chip); (2) Mensa [45], a heterogeneous edge NN inference accelerator, which uses 3D-stack-based PNM to speed up memory-bound NN models; and (3) SIMDRAM [206], a PUM architecture,

<sup>1</sup>There is no consensus on the terminology related to processing-in-memory in the current literature. However, we borrow the terms “processing-near-memory” (PNM) and “processing-using-memory” (PUM) from [75], which clearly defines these two terms and demonstrates that existing PIM techniques fall into one of these two categories.

which uses the analog properties of DRAM to execute bit-serial operations. These three *state-of-the-art* PIM architectures broadly cover the design space for PIM designs since (1) UPMEM represents the design of 2D-based PNM systems, (2) Mensa represents the design of a PNM system that leverages 3D-stacked integration to add specialized hardware units near DRAM, and (3) SIMDRAM represents the design of PUM systems.

We draw three key takeaways from our analysis. First, the evaluated PIM architectures provide significant performance improvement and energy savings for NN inference when compared against compute-centric architectures (i.e., CPUs, GPUs, and compute-centric edge TPUs). Second, there is *no* holy grail PIM architecture that can broadly accelerate *all* different types of NN models. This happens because different PIM architectures come with different trade-offs (e.g., limited memory capacity, high cost, high complexity of mapping workloads to the PIM substrate, lack of support for key operations in NN inference). However, regardless of the underlying operating principles of our three state-of-the-art PIM architectures, they all can alleviate the memory bottlenecks our evaluated NN models suffer from by leveraging the internal memory bandwidth and abundant parallelism available inside DRAM.

Third, there is a need for programming models and frameworks that can unify the benefits of the different PIM architectures into a single heterogeneous system. Such solutions need to map, schedule, and control the execution of NN models on the most appropriate PIM architecture. Thus, they can enable a workload to leverage the benefits of PIM while avoiding particular drawbacks related to a given PIM architecture. We conclude that PIM is a promising solution to improve the performance and energy efficiency of several NN models.

We make the following key contributions:

- We investigate how three PIM architectures can be used to improve the performance and energy efficiency of different NN models.
- We observe that the fundamental properties of the target PIM architecture define the most suitable type of NN model for the underlying architecture.

## Drawbacks of Compute-Centric NN Accelerators

We analyze the performance and energy of executing NN models using a commercial state-of-the-art compute-centric NN accelerator, called the Google Edge TPU [52], as our baseline accelerator. The Edge TPU has a generic tiled architecture, similar to other state-of-the-art accelerators [6, 63]. It includes a  $64 \times 64$  2D array of floating-point multiply-and-accumulate processing elements (PEs), where each PE has a small register file to hold intermediate results. The accelerator has two large SRAM-based on-chip buffers to hold model parameters (4 MB parameter buffer) and activations (2 MB activation buffer). We analyze 24 Google edge NN models, including convolutional neural networks (CNNs) [7–11], long short-term memory (LSTM) networks [19–21], transducers [36, 37], and recurrent convolutional neural networks (RCNNs) [26, 38, 39]. Based on our analysis, we find that the accelerator suffers from three key shortcomings.

**1. The accelerator often suffers from extreme underutilization of the PEs.** The Edge TPU has a theoretical peak throughput of 2 TFLOP/s. However, the accelerator operates at a throughput *much* lower than its peak throughput during inference execution (75.6% lower on average). Figure 1 (left) shows the throughput roofline model [207] for the Edge TPU, along with the measured throughput of all of our edge models. We observe that the PE utilization is low across all models. Transducer and LSTM models have the highest underutilization, with both achieving less than 1% of peak throughput. While CNN and RCNN models do somewhat better, they achieve only 40.7% of peak utilization on average (with a minimum of only 10.2% of peak utilization). We identify two main reasons why the actual throughput of the Edge TPU falls significantly below its peak.

First, while some layers have high parameter reuse (1200 FLOP/B ratio), other layers exhibit very low reuse (1–64 FLOP/B) while at the same time having large parameter footprints (0.5–5 MB). Layers with low reuse yet large parameter footprints are *memory-bound* and often leave PEs idle, as the parameters incur long-latency cache misses to DRAM.

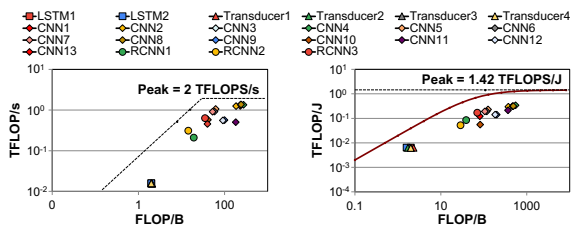


**Figure 1: Throughput roofline (left) and energy efficiency roofline (right) for the Edge TPU across all Google edge NN models.**

Second, the Edge TPU does *not* provide a custom dataflow optimized for each layer. From our analysis, we observe that layers both across and within models exhibit high variation in terms of data reuse patterns and computational intensity. This variation necessitates the need for *different* dataflows for different layers, where each dataflow exposes a different set of reuse opportunities for parameters and activations.

**2. The Edge TPU operates far below its theoretical maximum energy efficiency.** Figure 1 (right) shows the energy efficiency roofline [208] for the Edge TPU, along with the energy efficiency achieved for each model. On average across all models, the Edge TPU achieves only 37.2% of its maximum possible energy efficiency. The energy efficiency is particularly low (33.8% of the maximum) for LSTM and Transducer models, but even the best CNN model achieves only 50.7% of the maximum energy efficiency. To understand the accelerator’s low energy efficiency, we analyze (in Figure 2) the energy breakdown during inference execution across different models. We make three key observations.

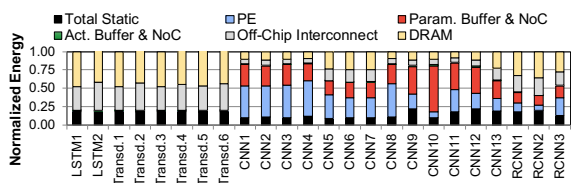


**Figure 2: Energy breakdown during inference.**

First, the on-chip buffers (the activation buffer and the parameter buffer) account for a significant portion of both static and dynamic energy across all models. Second, averaged across all models, the Edge TPU spends 50.3% of its total energy on off-chip memory accesses. Third, for LSTMs and Transducers, the Edge TPU spends approximately three quarters of its total energy on DRAM accesses. This is because while the buffers consume

a significant amount of area in the Edge TPU (79.4% of the total area), they are ineffective at reducing off-chip memory accesses.

**3. The accelerator’s memory system design is neither effective nor efficient.** The Edge TPU memory system, which includes both on-chip buffers and off-chip memory, is highly inefficient, and results in significant energy consumption.

**Key Takeaways.** Our analysis provides two key insights: (1) there is significant variation in terms of layer characteristics *across* and *within* edge NN models, where models vary from being compute-bound and memory-bound; (2) the monolithic design of state-of-the-art NN accelerators mainly caters for compute-bound NN models, which leads to high underutilization and low energy efficiency of memory-bound NN models.

### PIM Architectures for NN Inference

The *goal* of our work is to explore how different state-of-the-art PIM architectures<sup>2</sup> overcome the memory bottlenecks caused by data movement in NN inference in different environments (i.e., from edge devices to cloud servers).

We conduct our analysis in three steps. First, we evaluate the performance of a key primitive in NN inference (i.e., general matrix–vector multiplication, GEMV) on the first commercial server-based PIM architecture (UPMEM [88, 90–92, 204, 205]), which is a 2D general-purpose PNM architecture. Second, we design specialized NN inference accelerators for 24 different edge NN models in a 3D-stacked memory using the Mensa framework [45]. Since Mensa relies on the 3D integration of logic and memory, the micro-architecture for the PIM accelerators can consist of an extensive range of processing elements, including costly floating-point MAC units. Third, we map three different binary neural networks (BNNs) [41, 209–212] to a PUM substrate called SIMDAM [206], which is a promising solution for both edge-based and cloud-based systems since it operates using standard 2D DDRx DRAM chips. We conclude by drawing key takeaways from our analyses, and based on them, we provide some guidelines for future PIM systems targeting NN inference.

<sup>2</sup>We refer the reader to the sidebar for a brief discussion of several other related works.

These three *state-of-the-art* PIM architectures broadly cover the design space for general-purpose 2D PNM (UPMEM), specialized 3D PNM (Mensa), and DRAM-based PUM (SIMDRAM) proposals. Regardless of the underlying operating principles of our three state-of-the-art PIM architectures, they all leverage DRAM’s abundant internal parallelism and internal memory bandwidth to alleviate memory bottlenecks.

### NN Inference on General-Purpose 2D-Based Processing-near-Memory

We conduct a preliminary analysis of the potential of the first commercially-available server-based PIM system, called UPMEM [88, 90–92, 204, 205], for NN inference. Many NN inference workloads (e.g., CNN, LSTM) use matrix–vector multiplication (GEMV) as a key operation. GEMV is characterized as memory-bound in compute-centric architectures (i.e., CPU, GPU) [76, 92]. As a result, GEMV is a suitable candidate to be mapped onto the UPMEM architecture.<sup>3</sup> We compare quantitatively and qualitatively our PIM implementation of GEMV to its state-of-the-art GPU counterpart.

#### UPMEM PIM Architecture

Figure 3 (left) depicts an UPMEM-based PIM system with (1) a *host* CPU, (2) standard main memory (DRAM modules), and (3) PIM-enabled memory (UPMEM modules) [88]. An UPMEM module is a standard DDR4-2400 DIMM (module) with 16 PIM chips.

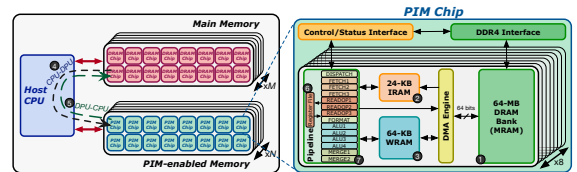


**Figure 3: UPMEM-based PIM system [88, 92].**

Inside each UPMEM PIM chip (Figure 3, right), there are 8 small general-purpose in-order processors, called *DPUs*. DPUs are fine-grained multithreaded. Each DPU has exclusive access to (1) a 64 MB DRAM bank, called *MRAM* ①; (2) a 24 kB instruction memory, called *IRAM* ②; and

<sup>3</sup>We show GEMV performance in our UPMEM experiments as a preliminary evaluation of the benefits the UPMEM system can provide for NN inference. Implementing an end-to-end NN inference model using the UPMEM system requires non-trivial effort, which we leave for future work.

(3) a 64 kB scratchpad memory, called *WRAM* ③. MRAM is accessible by the host CPU (Figure 3, left) for *copying* input data (from main memory to MRAM) ④ and *retrieving* results (from MRAM to main memory) ⑤. In UPMEM, data is explicitly copied from a CPU to DPUs, and from MRAM to WRAM using CPU instructions. The UPMEM runtime system transposes DPU data using software libraries so that a 64-bit word is placed inside a single DPU. There is no communication path across DPUs: all inter-DPU communication happens through the CPU. In current UPMEM-based PIM systems, the maximum number of UPMEM DIMMs is 20. Thus, the PIM system contains up to 2,560 DPUs which amounts to 160 GB of PIM-capable memory.

### Evaluation Methodology

We evaluate GEMV on a real UPMEM-based PIM cloud system with 2048 DPUs and on a state-of-the-art NVIDIA A100 GPU [213, 214]. We use an open-source implementation of GEMV for UPMEM [90–92] and the cuBLAS library [215] for the GPU. DPUs run at 428 MHz. The maximum aggregated memory bandwidth for 2048 DPUs is 1.7 TB/s for a memory capacity of 128 GB. The A100 GPU runs at 1.4 GHz. The A100 GPU features 40 GB of HBM2 memory [216] with a bandwidth of 1.5 TB/s.

We perform two experiments. First, we evaluate performance and scalability characteristics of GEMV on the UPMEM system. Second, we compare the performance of GEMV on 2048 DPUs with that on the GPU. Since the amount of memory of the GPU is relatively small, we evaluate one version with regular memory allocation and another version with unified memory allocation, which allows memory oversubscription.

### Results

Figure 4 shows strong scaling results of GEMV for four different matrix sizes on the UPMEM system. The matrices have 32-bit floating-point or integer values. The experiment uses 256, 512, 1024, and 2048 DPUs. Inside each DPU, we execute 16 software threads.

We make two observations. First, the execution with floating-point values takes one order of magnitude more time than the execution with integers. The reason is that the UPMEM DPUs

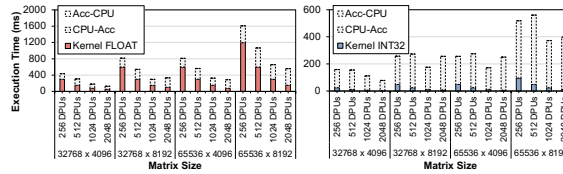


**Figure 4: Execution time (ms) of GEMV for 32-bit floating-point (left) and 32-bit integer (right) on 256, 512, 1024, and 2048 DPUs.**

do *not* have native support for floating-point operations. This is a limitation that comes from the difficulty of integrating logic into DRAM chips [217]. As a result, floating-point operations are emulated [92]. Second, the kernel execution time of GEMV (both floating-point and integer values) scales linearly on the UPMEM system. The DPU kernel execution time reduces by nearly 2× when we double the number of DPUs.

Figure 5 shows the comparison of GEMV (integer values) on the PIM system with 2048 DPUs to the A100 GPU. We observe that the GEMV kernel execution time on the 2048-DPU UPMEM system and on the GPU (without unified memory) is in the same order of magnitude, with the GPU being 4–5× faster than the UPMEM system. This is because (1) the peak compute throughput of the A100 GPU is orders of magnitude higher (TFLOPs vs. GOPs) even though the UPMEM system and the A100 GPU have similar memory bandwidth [92], and (2) 32-bit integer multiplication is emulated on the UPMEM DPUs (there is no 32-bit multiplier [88]).

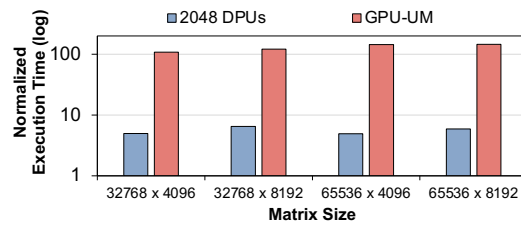


**Figure 5: Normalized execution time of GEMV for 32-bit integer values on 2048 DPUs and A100 GPU with unified memory (GPU-UM). Values are normalized to an A100 GPU without unified memory.**

There are three key takeaways from this comparison. First, the GPU has significant compute resources (including hardware multipliers), which leads to its higher performance. As future PIM systems integrate better (e.g., higher precision)

multipliers and more compute resources as GPUs have done, we expect their performance to get significantly higher. Second, the GEMV kernel is very memory-bound on GPU for large matrix sizes. In contrast, the UPMEM system balances GEMV’s compute and memory requirements better. Third, when employing a unified memory allocation in the GPU system, the GEMV kernel’s execution time increases significantly. In this case, *both* the 2048-DPU system and the GPU without unified memory greatly outperform the GPU with unified memory. Allowing memory oversubscription in the GPU has a large performance cost due to overheads related to address translation and page swapping between the CPU and GPU memories [218–220]. The UPMEM system avoids the need for a unified memory space, since it provides higher memory capacity and better scalability of computing throughput and memory size compared to the GPU.

We run one final experiment (not shown in the figure) where we compare GEMV on the UPMEM system for 32-, 16-, and 8-bit integers. The DPU contains an 8-bit multiplier [88], which allows the 16-bit and the 8-bit versions to be  $1.75\times$  and  $2.17\times$  faster than the 32-bit version, respectively. These results demonstrate the potential of the UPMEM system for NN inference in cases where fixed-point computation and quantization are feasible, despite the inherent limitations derived from the integration of logic units inside the 2D DRAM chip.

## NN Inference on Specialized 3D-Based Processing-near-Memory

Modern 3D-stacked memories [221–223] such as High Bandwidth Memory [221] and the Hybrid Memory Cube [222] include logic layers that have access to the high memory bandwidth available within a 3D-stacked memory chip [75]. We evaluate the opportunities a 3D-stack-based PNM architecture provides for NN inference. To do so, we use Mensa [45], a new machine learning accelerator design framework that distributes the layers from an NN model across a collection of smaller memory- and compute-centric hardware accelerators that are specialized to the properties of different NN layer types. By specializing each accelerator to a subset of NN layers, Mensa avoids the shortcomings of monolithic edge NN

accelerators, resulting in a highly-efficient and high-performance heterogeneous accelerator with a much smaller area footprint.

We employ Mensa’s methodology to design a specialized NN inference system for the Google edge NN models discussed in our motivation. For each layer, we study the correlation between different characteristics. These characteristics include (1) parameter reuse (FLOP/B), (2) parameter footprint (MB), and (3) MAC intensity (defined by the number of MAC operations). Based on all of the layer characteristics that we analyze, we observe across all layers from all models that 97% of the layers group into one of five layer families. We design different accelerators to cater to the properties of each layer family.

We identify that (a) layers in Families 1 and 2 share a high MAC intensity (20M–20M), small parameter footprint (1–500 kB), and moderate-to-high parameter reuse (81–20K FLOP/B); while (b) layers in Families 3 and 4 share a low MAC intensity (0.1M–25M), large parameter footprint (0.5–18 MB), and low parameter reuse (1–64 FLOP/B). Thus, we need *at least* two different accelerator designs: one that caters to the compute-centric behavior of Families 1/2, and one that caters to the data-centric behavior of Families 3/4. Given our resource-constrained edge environment, we look to see if layers in Family 5, which have a low MAC intensity (similar to Families 3 and 4) but a relatively small parameter footprint (similar to Families 1 and 2), can benefit from one of these two approaches. We find that the low MAC intensity, along with the low parameter reuse by many Family 5 layers, allow the layers to benefit from many of the data-centric optimizations that benefit Families 3 and 4, so we study Families 3/4/5 collectively as we design the data-centric accelerators.

Figure 6 shows the design of the three Mensa accelerators, called Pascal, Pavlov, and Jacquard, which we collectively refer to as Mensa-G. We tailor the hardware components (i.e., PE array size, on-chip parameter and activation buffers size, accelerator placement) and dataflow for each accelerator based on the properties of the layer families it targets. We briefly describe the hardware components of each accelerator next. We refer the reader to the full Mensa paper [45] for a detailed description of each accelerator.

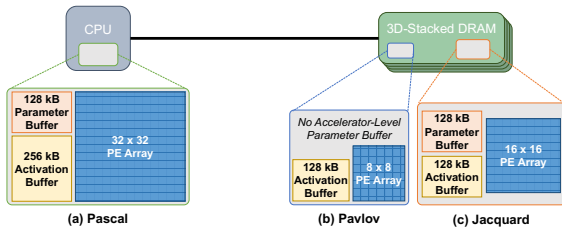


Figure 6: Mensa-G accelerator design.

**Pascal: Compute-Centric Accelerator Design.** Pascal caters to layers in Families 1 and 2, which are compute-centric. We design Pascal as shown in Figure 6a. First, the PE array in Pascal needs to have enough PEs to accommodate the high MAC intensity exhibited by layers in Families 1 and 2. Thus, we profile the performance of Family 1/2 layers on different PE sizes and empirically choose a  $32 \times 32$  PE array, which lets Pascal achieve a 2 TFLOP/s peak throughput. Second, we reduce the size of the activation buffer from 2 MB in the Edge TPU to 256 kB (i.e., by  $8 \times$ ) in Pascal, because Pascal’s dataflow exploits temporal reduction for the output activations using the internal PE registers, and no longer needs to store the large footprint of the output activations in the activation buffer. We reduce the size of the parameter buffer from 4 MB in the Edge TPU to 128 kB in Pascal, because layers in Families 1 and 2 have small parameter footprints. Given the low off-chip memory bandwidth requirements of Pascal, we keep the accelerator on the CPU die.

Pascal’s dataflow reduces memory traffic by enabling two types of reuse. First, the dataflow uses temporal reduction [224] for each output activation element, by having a single PE accumulate the entire sum of the elements across multiple cycles in the PE’s register file. Second, the dataflow uses spatial multicasting [224] for each parameter, by ensuring that all PEs work on the same image channel<sup>4</sup> in the same cycle.

**Pavlov: Data-Centric Accelerator Design for (Mainly) LSTMs.** Pavlov caters to layers in Family 3, which are data-centric *and* predominantly consist of LSTM layers. We design Pavlov as shown in Figure 6b. First, because Family 3 layers have low MAC intensity, we empirically choose a small  $8 \times 8$  PE array for Pavlov.

<sup>4</sup>A layer in a CNN can sometimes break down an input into multiple filtered channels (e.g., breaking an image down into red, green, and blue colors).

This allows Pavlov to achieve 128 GFLOP/s peak throughput. Second, we place Pavlov *inside memory* to accommodate the significant off-chip memory bandwidth requirements of Family 3 layers. Given that parameters and activations from Family 3 layers exhibit different characteristics, for parameters, we use only one level of memory hierarchy (512B of private registers per PE), eliminating the parameter buffer, and streaming parameters directly from DRAM. The per-PE registers provide enough space to cache the temporally-multicasted parameters, and there are no other reuse opportunities that the parameter buffer could exploit. Thanks to the small activation footprint of Family 3 layers, we use a 128 kB buffer for activations ( $16 \times$  reduction over the Edge TPU’s activation buffer).

Pavlov’s dataflow reduces memory traffic by enabling two types of reuse. First, the dataflow temporally reuses a weight by allowing the PEs to store the weight and partial sums in one of their private registers. Second, the dataflow uses spatial multicasting for each input activation, as the same activation is multiplied across all columns for a given row of a parameter matrix.

**Jacquard: Data-Centric Accelerator Design for (Mainly) Non-LSTM NNs.** Jacquard caters to layers in Families 4 and 5, which primarily consist of non-LSTM data-centric layers. We design Jacquard as shown in Figure 6c. First, while layers in Families 4 and 5 have low MAC intensity, they perform more MAC operations on average than Family 3 layers. Thus, we empirically select a  $16 \times 16$  PE array for Jacquard. This allows Jacquard to achieve a peak throughput of 512 GFLOP/s. Second, similar to Pavlov, we place Jacquard inside the logic layer of 3D-stacked memory. Doing so enables high memory bandwidth for the large parameter footprints of Family 4 layers. Given the small activation footprints, we use a small 128 kB buffer for them (a  $16 \times$  reduction compared to the Google Edge TPU). Thanks to the temporal parameter reuse that Jacquard’s dataflow enables, we reduce the parameter buffer to 128 kB (a  $32 \times$  reduction compared to the Google Edge TPU).

Jacquard’s dataflow reduces memory traffic by enabling two types of reuse. First, the dataflow temporally reuses parameters. As in Pavlov, a parameter is stored in a PE register and reused over

multiple cycles to reduce the number of times the parameter is fetched from memory. By increasing the reuse of the parameter, the dataflow hides the off-chip memory access latency by overlapping it with PE computation. Second, the dataflow uses spatial multicasting for each input activation. To enable spatial multicasting for Families 4 and 5, the dataflow enables all PEs to collectively compute a single output activation in two steps. In the first step, each PE computes a partial sum. In the second step, the on-chip interconnect is used to gather partial sums from all PEs and produce the final output activation.

**Layer-to-Accelerator Mapping.** We design a software runtime scheduler to identify which accelerator each layer in an NN model should run on. When an NN model runs on Mensa, the scheduler maps each NN layer to different accelerators. The scheduler uses the NN model (including a directed acyclic graph representing communication across model layers) and the configuration information in the accelerator hardware driver to determine this mapping.

**Execution and Communication.** Once the layer-to-accelerator mapping is complete, Mensa begins model execution. During execution, destination layer  $i$  placed in accelerator  $j$  needs to read (1) any unbuffered parameters (i.e., weights) from DRAM; and (2) input activations (i.e., input data) produced by layer  $i - 1$ , when layer  $i$  is run on a different accelerator than  $j$ . In order to simplify communication between accelerators, Mensa accelerators transfer activations to another accelerator through DRAM, avoiding the need to keep on-chip data coherent across accelerators (or, when some of the Mensa accelerators are placed near memory, to keep on-chip and near-data accelerators coherent [45, 64, 123, 134]).

### Evaluation Methodology

We evaluate end-to-end inference energy (using an energy model based on prior works [63, 64]), hardware utilization, and throughput (using an in-house simulator)<sup>5</sup> of three configura-

<sup>5</sup>We implement Mensa using Google’s Edge TPU in-house simulator as a base, which faithfully models all major components of the Google Edge TPU, including the PE array, memory system, on-chip network, and dataflow. In our in-house simulator, the logic layer of 3D-stacked memory accelerators has access to the 256 GB/s internal bandwidth of High Bandwidth Memory (HBM) [221], which is  $8\times$  the external memory bandwidth of accelerators that sit outside of memory.

tions: (1) *Baseline*, the Google Edge TPU [52]; (2) *Base+HB*, a hypothetical version of *Baseline* with  $8\times$  the memory bandwidth (256 GB/s), similar to monolithic 3D-stack-based PNM inference accelerators [63]; and (3) *Mensa-G* with all three accelerators (Pascal, Pavlov, Jacquard).

### Results

**Energy Analysis.** Figure 7 shows the total inference energy consumed by the three systems we evaluate across different NN models. We report results for representative LSTM, Transducers, CNNs, and RCNNs to improve the figure’s clarity. We report average energy values for all 24 Google edge NN models. We make two observations.

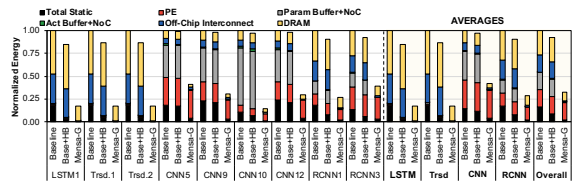


**Figure 7: Inference energy across different models normalized to Baseline.**

First, providing high memory bandwidth to *Baseline* (*Base+HB*) results in only a small reduction in energy (7.5% on average). This is because *Base+HB* still incurs a high energy cost due to (1) on-chip buffers that are overprovisioned for many layers, and (2) off-chip traffic to DRAM. Second, *Mensa-G* significantly reduces energy across all models. The reduction primarily comes from three sources. (1) *Mensa-G* lowers the energy spent on on-chip and off-chip parameter traffic by  $15.3\times$  over *Baseline*, by scheduling each layer on the accelerator with the most appropriate design and dataflow for that layer. LSTMs and Transducers benefit the most, as their energy in *Base+HB* is dominated by off-chip parameter traffic, which Pavlov and Jacquard drastically reduce by being placed inside memory. (2) *Mensa-G* reduces the dynamic energy of the on-chip buffer and on-chip network (NoC) by  $49.8\times$  over *Base+HB* by avoiding overprovisioning and catering to specialized dataflows. This is most beneficial for CNN and RCNN models. (3) *Mensa-G* reduces static energy by  $3.6\times$  over *Base+HB* thanks to using significantly smaller PE arrays that avoid underutilization, significantly smaller on-chip buffers, and dataflows that reduce inference latency.



**Utilization and Throughput Analyses.** Figure 8 shows the raw PE utilization (top) and *Baseline*-normalized throughput (bottom) for our three configurations. *Mensa-G*’s utilization is calculated by computing the average utilization across its three accelerators (Pascal, Pavlov, and Jacquard). We make two observations.

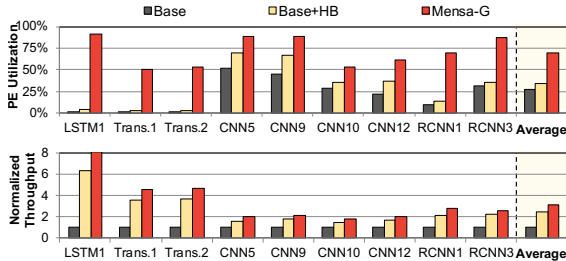


**Figure 8: PE utilization (top) and *Baseline*-normalized throughput (bottom).**

First, *Baseline* suffers from low PE array utilization (on average 27.3%). The higher memory bandwidth in *Base+HB* increases the average PE utilization to 34.0%, and improves throughput by 2.5 $\times$ . Overall, *Base+HB* still has very low utilization, as many layers (those from Families 3, 4, and 5) do *not* need the large number of PEs in the accelerator. Second, *Mensa-G* significantly increases both average utilization (by 2.5 $\times$ /2.0 $\times$ ) and throughput (by 3.1 $\times$ /1.3 $\times$ ) over *Baseline/Base+HB*. The large utilization improvements are a result of (1) properly-provisioned PE arrays for each layer, (2) customized dataflows that exploit reuse and opportunities for parallelization, and (3) the movement of large-footprint layer computation into 3D-stacked memory (which eliminates off-chip traffic for their DRAM requests).

## NN Inference on Processing-using-Memory

A common approach for PUM architectures is to make use of bulk bitwise computation. *Ambit* [167, 168, 171, 179, 180, 182], a DRAM-based PUM architecture, was the first work to propose exploiting DRAM’s analog operation to perform bulk bitwise AND, OR, and NOT logic operations. *Ambit* leverages the fact that by simultaneously accessing three DRAM rows, the DRAM row sensing circuitry pulls its output voltage level to the majority voltage level among the three accessed rows, performing a majority-of-three (MAJ) operation. AND and OR logic

operations can be performed by setting one of the three simultaneously accessed DRAM rows to either ‘1’ (for an OR) or ‘0’ (for an AND). To implement NOT, *Ambit* uses and feeds into a DRAM array the complemented value of a cell that already exists after sensing in the sense amplifier. *SIMDRAM* [206] builds on top of *Ambit* to implement complex operations efficiently in DRAM using an end-to-end framework. Such a framework efficiently implements arbitrary in-DRAM operations by (1) leveraging MAJ/NOT-based computation (instead of *Ambit*’s focus on AND/OR/NOT-based computation) and (2) by employing a bit-serial execution model.

*SIMDRAM* consists of three key steps to enable any desired operation in DRAM: (1) building an efficient MAJ/NOT-based representation of the desired operation, (2) mapping the operation’s input and output operands to DRAM rows and to the required DRAM commands that produce the desired operation, and (3) executing the operation. These three steps ensure efficient computation of a wide range of arbitrary and complex operations in DRAM. The first two steps give users the flexibility to efficiently implement and compute any desired operation in DRAM. The third step controls the execution flow of the in-DRAM computation, transparently from the user.

For a desired computation, the first step derives its optimized MAJ/NOT-based implementation from its AND/OR/NOT-based implementation. The second step translates the MAJ/NOT-based implementation into DRAM row activations. This step includes (1) mapping the operands to the designated rows in DRAM, and (2) defining the sequence of DRAM row activations that are required to perform the computation. *SIMDRAM* chooses the operand-to-row mapping and the sequence of DRAM row activations to minimize the number of DRAM row activations required for a specific operation. To this end, we present a new row allocation algorithm inspired by the linear scan register allocation algorithm [225]. However, unlike register allocation algorithms, our row allocation algorithm considers two extra constraints that are specific to processing-using-DRAM: (1) performing MAJ in DRAM has destructive behavior; and (2) the number of DRAM rows that are designated to perform bitwise operations is limited. The third

step programs the memory controller to issue the sequence of DRAM row activations to the appropriate rows in DRAM to perform the computation specified by the operation. To this end, SIMD RAM uses a control unit in the memory controller that user-transparently executes the sequence of DRAM row activations for each specific operation.

We use SIMD RAM to efficiently support a wide range of operations of different types. We implement a set of 16 SIMD RAM operations of five different types for  $n$ -bit data elements: (1)  $N$ -input logic operations (OR-/AND-/XOR-reduction across  $N$  inputs); (2) relational operations (equality/inequality check, greater-/less-than check, greater-than-or-equal-to check, and maximum/minimum element in a set); (3) arithmetic operations (addition, subtraction, multiplication, division, and absolute value); (4) predication (if-then-else); and (5) other complex operations (bit-count, and ReLU [226]). We support four element sizes that correspond to data type sizes in popular programming languages (8-/16-/32-/64-bit integers).

### System Integration

A program in a SIMD RAM-enabled system can have a combination of CPU and SIMD RAM instructions, with possible data sharing between the two. This leads to several challenges in integrating SIMD RAM into a real system. We discuss two system integration challenges related to data mapping and internal memory communication. The full SIMD RAM paper [206] contains further discussion about other system integration challenges and how we address them, including (1) data layout and how SIMD RAM stores the data required for in-DRAM computation in a vertical layout and transposes such data when it is needed in a horizontal layout; (2) ISA extensions for and programming interface of SIMD RAM; (3) how SIMD RAM handles page faults, address translation, coherence, and interrupts; (4) how SIMD RAM manages computation on large amounts of data; (5) security implications of SIMD RAM; and (6) current limitations of SIMD RAM.

**Data Mapping.** SIMD RAM uses a special ISA instruction (`bbop_trsp_init`) to inform the operating system (OS) that a memory location

is a SIMD RAM object. This allows the OS to perform virtual-to-physical memory mapping optimizations for the SIMD RAM object before the allocation starts (e.g., mapping the arguments of an operation to the same row/column in physical memory).

**Internal Communication.** SIMD RAM does *not* support communication across different in-DRAM SIMD lanes (i.e., there is no communication across DRAM bitlines). Communication across subarrays and banks can be performed using prior works (i.e., LISA [227] and Row-Clone [170], respectively).

### Evaluation Methodology

We map three different binary neural networks (BNNs) [41, 209–212] to our PUM substrate since SIMD RAM operates in a bit-serial model and only supports integer operations. BNNs are CNNs whose activations and weights are represented with 1-bit values, enabling convolutions by executing bit-serial bitcount, shift, and addition operations [186]. We use the XNOR-NET [41] implementations of VGG-13, VGG-16, and LeNET provided by [186], to evaluate the functionality of SIMD RAM. We modify these implementations to make use of SIMD RAM’s bitcount, addition, shift, and XNOR operations. We evaluate all three networks for inference using two different datasets: CIFAR-10 [228] (for VGG-13 and VGG-16), and MNIST [229] (for LeNet-5). We evaluate BNN inference time in SIMD RAM by isolating the main kernel that SIMD RAM executes (i.e., bitwise convolution) and evaluating its performance. We estimate the end-to-end speedup SIMD RAM provides for each BNN by applying Amdahl’s law [230]. Thus, SIMD RAM’s end-to-end speedup is given by:  $((1 - conv\_time) + \frac{conv\_time}{SIMDRAM\_speedup})^{-1}$ ; where  $SIMDRAM\_speedup$  is the speedup SIMD RAM provides for the main kernel compared to the CPU execution, and  $conv\_time$  is the percentage of the total execution time the main kernel represents when executing BNN inference on the baseline CPU.

We implement SIMD RAM using the gem5 simulator [231] and compare it to a real multicore CPU (Intel Skylake [232]), a real high-end GPU (NVIDIA Titan V [233]), and a state-of-the-art processing-using-DRAM mecha-

nism (Ambit [167, 168, 171, 179, 180, 182]). We validate our Ambit and SIMDRAM gem5 implementations rigorously with the results reported in the original Ambit paper. We evaluate three different configurations of SIMDRAM where 1 (*SIMDRAM:1*), 4 (*SIMDRAM:4*), and 16 (*SIMDRAM:16*) DRAM banks out of all the 16 banks in one channel have SIMDRAM computation capability. *SIMDRAM:1*'s throughput for bitcount, addition, shift, and XNOR operations used during BNN inference are 24.3 GOPs/s, 20.1 GOPs/s, 1337.5 GOPs/s, and 51.4 GOPs/s, respectively, and this throughput scales linearly with the number of DRAM banks.

## Results

Figure 9 shows the performance of SIMDRAM, the GPU, and Ambit for each BNN, normalized to that of the multicore CPU. We make two observations.

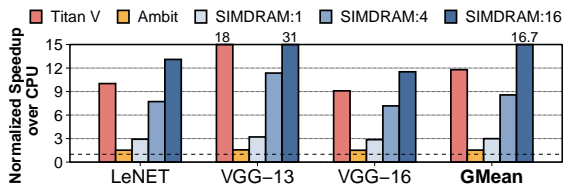


**Figure 9: Normalized speedup of 3 BNNs.**

First, *SIMDRAM:16* greatly outperforms the CPU and GPU baselines, providing  $16.7\times$  and  $1.4\times$  the performance of the CPU and GPU, respectively, on average across all three NNs. SIMDRAM has a maximum performance of  $31\times$  and  $1.7\times$  that of the CPU and GPU, respectively (for VGG-13 in both cases). Similarly, *SIMDRAM:1* provides  $1.9\times$  the performance of Ambit (which also uses a single bank for in-DRAM computation), on average across all three NNs, with a maximum of  $2\times$  the performance of Ambit for VGG-13. Second, even with a single DRAM bank, SIMDRAM *always* outperforms the CPU baseline, providing  $3\times$  the performance of the CPU on average across all NNs. We conclude that SIMDRAM is an effective and efficient substrate to accelerate NN inference.

## Key Takeaways and Future Opportunities

This article investigates the benefits of state-of-the-art PIM architectures in mitigating memory bottlenecks during NN inference. We identify

the key opportunities and challenges for three PIM solutions that can be employed in edge or cloud environments. We summarize the key takeaways from our analysis as follows.

First, we evaluate the performance of the GEMV primitive, which is a key operation for NN inference, on a commercial general-purpose server-scale PNM architecture (UPMEM) using 32-bit floating-point and integer data types. Our experiments allow us to gain insights on the benefits a *real* PIM architecture can provide for NN inference. We observe that while GEMV using floating point takes one order of magnitude more time than using integers, the kernel execution time scales linearly with the number of UPMEM processing cores employed. When considering the 32-bit integer GEMV implementation, the UPMEM system provides similar performance to a high-end GPU, even outperforming the GPU when the GPU requires memory oversubscription. There are two key benefits of the UPMEM system compared to the other two PIM systems. (1) It is relatively *easy to scale* the UPMEM system to higher memory capacities and computational power by simply adding more UPMEM modules to a system. In contrast, scaling the 3D-stack-based PNM architecture requires non-trivial engineering since 3D memory cubes need to be connected using specialized interconnection network. (2) It is relatively *easy to program* the UPMEM system since UPMEM provides a complete programming toolkit and a C-based programming model for their system. In contrast, for the PUM architecture, the programmer needs to manually map a workload to the underlying substrate, which is an arduous task.

Second, Mensa, a heterogeneous architecture for Google edge NN models that employs 3D-based PNM, greatly benefits many NN models, improving performance (throughput and utilization) and energy efficiency, while at the same time reducing the area footprint of the monolithic Google Edge TPU. The key benefit of Mensa's 3D-based PNM accelerator compared to the 2D-based PIM designs we evaluate (SIMDRAM and UPMEM) is its *flexibility*. Since the logic and memory components of a 3D-based architecture are separately manufactured, the design of a near-memory accelerator has no constraints other than the area and power constraints of the logic layer.

This means that, in practice, the 3D-based architecture can accelerate many NN types relatively flexibly. In contrast, 2D PNM and PUM have natural limitations that make them infeasible or unsuitable to support floating-point computation, which is standard for most NN operations. The key drawback of PNM solutions that rely on 3D-stacked memories is the *high cost* and *limited memory capacity* associated with 3D memories. This can be a limiting factor in edge environments (since edge devices are often cost-sensitive) and future NN models (since NN model sizes are increasing significantly).

Third, SIMDRAM, a 2D-based PUM architecture, provides significant performance improvements for binary neural networks compared to high-end CPUs and GPUs. The key benefit of employing a PUM architecture for NN inference is the *massive parallelism* available inside DRAM. SIMDRAM's throughput for a 32-bit addition using a single DRAM bank is  $2.3\times$  that of a CPU [206] and scales linearly with the number of DRAM banks (up to  $36.8\times$  the CPU throughput using all 16 DRAM banks in a DRAM chip [206]) with relatively low area cost (i.e., only 0.2% area overhead in a high-end CPU). SIMDRAM is suitable for edge-based and cloud-based environments since it leverages the operating principles of standard DRAM DDRx memories. The key drawback of SIMDRAM is its *limited applicability* for NN models due to the lack of (1) support for floating-point operations and (2) tools (e.g., compilers, programming models) to map NN execution to the underlying hardware substrate.

We believe that there are many opportunities to improve the design of PIM architectures (both 2D and 3D) targeting NN inference, including better manufacturing processes that can seamlessly integrate logic and memory units, cheaper and efficient interconnection networks that can be used to scale up the capacity of 3D-based DRAM systems, and programming support to ease the deployment of PUM approaches. Also, there is a need for programming models and frameworks that can *unify* the benefits of the different PIM architectures into a single heterogeneous system. Such solutions need to map, schedule, and control the execution of different NNs onto the most appropriate PIM architecture, thereby enabling a

### Sidebar: Related Works on Accelerating NN Inference with Processing-in-DRAM

**2D PNM.** Beyond UPMEM, other memory manufacturers have announced PNM prototypes using 2D DRAM. Samsung's AxDIMM [1] integrates reconfigurable logic to DDR4 modules to accelerate recommendation systems. SK Hynix's GDDR6-based PIM [2] adds MAC units near DRAM banks to accelerate NN inference. Both solutions are not yet available on the market.

**3D PNM.** There is extensive literature on accelerating NN inference using 3D-stack-based PNM [3]. We highlight Samsung's FIMDRAM [4], an industry proposal (not yet available on the market) that adds MAC units near DRAM banks in an HBM2 device. A common drawback of prior 3D PNM NN accelerators is that they use a monolithic accelerator design, which cannot efficiently accommodate diverse types of NNs. Mensa avoids such issues by tailoring NN accelerators for the needs of different NN models.

**PUM.** DRISA [5] executes bulk operations in DRAM by adding logic elements inside DRAM arrays, providing speedups for binary neural networks. However, adding such logic to the DRAM array incurs large overheads. DrAcc [6] implements in-DRAM addition operations using AND/OR/NOT logic primitives, targeting ternary neural networks. SIMDRAM supports a wider range of operations (compared to DrAcc) at lower area overhead (compared to DRISA).

### REFERENCES

1. L. Ke *et al.*, "Near-Memory Processing in Action: Accelerating Personalized Recommendation with AxDIMM," *IEEE Micro*, 2021.
2. S. Lee *et al.*, "A 1ynm 1.25V 8Gb, 16Gb/s/pin GDDR6-Based Accelerator-in-Memory Supporting 1 TFLOPS MAC Operation and Various Activation Functions for Deep-Learning Applications," in *ISSCC*, 2022.
3. A. S. Cordeiro *et al.*, "Efficient Machine Learning Execution with Near-Data Processing," *MICPRO*, 2022.
4. Y.-C. Kwon *et al.*, "A 20nm 6GB Function-in-Memory DRAM, Based on HBM2 with a 1.2 TFLOPS Programmable Computing Unit Using Bank-Level Parallelism, for Machine Learning Applications." in *ISSCC*, 2021.
5. S. Li *et al.*, "DRISA: A DRAM-Based Reconfigurable In-Situ Accelerator," in *MICRO*, 2017.
6. Q. Deng *et al.*, "DrAcc: A DRAM Based Accelerator for Accurate CNN Inference," in *DAC*, 2018.

workload to leverage the benefits of PIM while avoiding particular drawbacks related to a given PIM architecture. We hope that our work brings attention to such challenges and can inspire future PIM system designs.

## Conclusion

We analyze, discuss, and contrast the benefits and drawbacks that different DRAM-based PIM architectures provide for NN performance and energy efficiency. To do so, we analyze three state-of-the-art PIM architectures, which broadly cover the PIM design space. Our comprehensive analysis provides several key takeaways. We conclude that while different PIM architectures provide greater performance and energy benefits than compute-centric solutions, different PIM architectures impose different limitations for NN workloads. We hope that our analysis can highlight the opportunities and drawbacks of state-of-the-art PIM solutions and inspire future designs.

## References

1. F. Rosenblatt, "The Perceptron: A Probabilistic Model for Information Storage and Organization in the Brain," *Psychological Review*, 1958.
2. A. G. Ivakhnenko and V. G. Lapa, *Cybernetic Predicting Devices*. CCM Information Corporation, 1965.
3. B. Yegnanarayana, *Artificial Neural Networks*. PHI Learning Pvt. Ltd., 2009.
4. T. P. Oliveira, J. S. Barbar, and A. S. Soares, "Computer Network Traffic Prediction: A Comparison between Traditional and Deep Learning Neural Networks," *IJBFI*, 2016.
5. Q. K. Al-Shayea, "Artificial Neural Networks in Medical Diagnosis," *IJCSI*, 2011.
6. V. Sze, Y.-H. Chen *et al.*, "Efficient Processing of Deep Neural Networks: A Tutorial and Survey," *Proceedings of the IEEE*, 2017.
7. K. Fukushima, "Neocognitron: A Self-Organizing Neural Network Model for a Mechanism of Pattern Recognition Unaffected by Shift in Position," *Biological Cybernetics*, 1980.
8. Y. LeCun, "Une Procédure d'Apprentissage pour Réseau à Seuil Asymétrique," in *Cognitiva*, 1985.
9. D. Rumelhart, G. E. Hinton, and R. J. Williams, "Learning Representations by Back-Propagating Errors," *Nature*, 1986.
10. Y. LeCun, Y. Bengio, and G. Hinton, "Deep Learning," *Nature*, 2015.
11. K. Simonyan and A. Zisserman, "Very Deep Convolutional Networks for Large-Scale Image Recognition," in *ICLR*, 2015.
12. J. Gu, Z. Wang *et al.*, "Recent Advances in Convolutional Neural Networks," *Pattern Recognition*, 2018.
13. Y. LeCun, B. Boser *et al.*, "Handwritten Digit Recognition with a Back-Propagation Network," in *NeurIPS*, 1989.
14. Y. LeCun, L. Bottou *et al.*, "Gradient-Based Learning Applied to Document Recognition," *Proc. IEEE*, 1998.
15. O. Russakovsky, J. Deng *et al.*, "ImageNet Large Scale Visual Recognition Challenge," *IJCV*, 2015.
16. M. D. Zeiler and R. Fergus, "Visualizing and Understanding Convolutional Networks," in *ECCV*, 2014.
17. C. Szegedy, W. Liu *et al.*, "Going Deeper with Convolutions," in *CVPR*, 2015.
18. K. He, X. Zhang *et al.*, "Deep Residual Learning for Image Recognition," in *CVPR*, 2016.
19. S. Hochreiter and J. Schmidhuber, "Long Short-Term Memory," *NECO*, 1997.
20. F. Gers, J. Schmidhuber, and F. Cummins, "Learning to Forget: Continual Prediction with LSTM," in *ICANN*, 1999.
21. K. Greff, R. K. Srivastava *et al.*, "LSTM: A Search Space Odyssey," *TNNLS*, 2017.
22. H. Sak, A. W. Senior, and F. Beaufays, "Long Short-Term Memory Based Recurrent Neural Network Architectures for Large Vocabulary Speech Recognition," arXiv:1402.1128 [cs.NE], 2014.
23. A. Graves, "Generating Sequences with Recurrent Neural Networks," arXiv:1308.0850 [cs.NE], 2013.
24. Y. Wu, M. Schuster *et al.*, "Google's Neural Machine Translation System: Bridging the Gap Between Human and Machine Translation," arXiv:1609.08144 [cs.CL], 2016.
25. K. Cho, B. Van Merriënboer *et al.*, "Learning Phrase Representations Using RNN Encoder-Decoder for Statistical Machine Translation," arXiv:1406.1078 [cs.CL], 2014.
26. J. Donahue, L. A. Hendricks *et al.*, "Long-Term Recurrent Convolutional Networks for Visual Recognition and Description," in *CVPR*, 2015.
27. A. Karpathy and L. Fei-Fei, "Deep Visual-Semantic Alignments for Generating Image Descriptions," in *CVPR*, 2015.
28. M. Ranzato, A. Szlam *et al.*, "Video (Language) Modeling: A Baseline for Generative Models of Natural Videos," arXiv:1412.6604 [cs.LG], 2014.
29. N. Srivastava, E. Mansimov, and R. Salakhudinov, "Unsupervised Learning of Video Representations Using LSTMs," in *ICML*, 2015.
30. I. Sutskever, O. Vinyals, and Q. V. Le, "Sequence to Sequence Learning with Neural Networks," in *NeurIPS*, 2014.

31. K. Xu, J. Ba *et al.*, "Show, Attend and Tell: Neural Image Caption Generation with Visual Attention," in *ICML*, 2015.
32. S. Xingjian, Z. Chen *et al.*, "Convolutional LSTM Network: A Machine Learning Approach for Precipitation Nowcasting," in *NeurIPS*, 2015.
33. J. Chung, C. Gulcehre *et al.*, "Empirical Evaluation of Gated Recurrent Neural Networks on Sequence Modeling," in *NeurIPS*, 2014.
34. S. Kanai, Y. Fujiwara, and S. Iwamura, "Preventing Gradient Explosions in Gated Recurrent Units," in *NeurIPS*, 2017.
35. K. Cho, B. Van Merriënboer *et al.*, "On the Properties of Neural Machine Translation: Encoder–Decoder Approaches," arXiv:1409.1259 [cs.CL], 2014.
36. A. Graves, "Sequence Transduction with Recurrent Neural Networks," in *ICML Representation Workshop*, 2012, arXiv:1211.3711 [cs.NE].
37. Y. He, T. N. Sainath *et al.*, "Streaming End-to-End Speech Recognition for Mobile Devices," in *ICASSP*, 2019.
38. M. Liang and X. Hu, "Recurrent Convolutional Neural Network for Object Recognition," in *CVPR*, 2015.
39. P. Pinheiro and R. Collobert, "Recurrent Convolutional Neural Networks for Scene Labeling," in *ICML*, 2014.
40. O. Vinyals, A. Toshev *et al.*, "Show and Tell: A Neural Image Caption Generator," in *CVPR*, 2015.
41. M. Rastegari, V. Ordonez *et al.*, "XNOR-Net: ImageNet Classification Using Binary Convolutional Neural Networks," in *ECCV*, 2016.
42. V. Vanhoucke, A. Senior, and M. Z. Mao, "Improving the Speed of Neural Networks on CPUs," <http://audentia-gestion.fr/Recherche-Research-Google/37631.pdf>, 2011.
43. A. Jain, M. A. Laurenzano *et al.*, "Architectural Support for Convolutional Neural Networks on Modern CPUs," in *PACT*, 2018.
44. R. Adolf, S. Rama *et al.*, "Fathom: Reference Workloads for Modern Deep Learning Methods," in *IISWC*, 2016.
45. A. Boroumand, S. Ghose *et al.*, "Google Neural Network Models for Edge Devices: Analyzing and Mitigating Machine Learning Inference Bottlenecks," in *PACT*, 2021.
46. N. P. Jouppi, C. Young *et al.*, "In-Datcenter Performance Analysis of a Tensor Processing Unit," in *ISCA*, 2017.
47. V. J. Reddi, C. Cheng *et al.*, "MLPerf Inference Benchmark," in *ISCA*, 2020.
48. S. Wang, A. Pathania, and T. Mitra, "Neural Network Inference on Mobile SoCs," *IEEE Design & Test*, 2020.
49. Y. Wang, G.-Y. Wei, and D. Brooks, "A Systematic Methodology for Analysis of Deep Learning Hardware and Software Platforms," in *MLSys*, 2020.
50. Y. E. Wang, G.-Y. Wei, and D. Brooks, "Benchmarking TPU, GPU, and CPU Platforms for Deep Learning," arXiv:1907.10701 [cs.LG], 2019.
51. U. Gupta, X. Wang *et al.*, "The Architectural Implications of Facebook's DNN-Based Personalized Recommendation," in *HPCA*, 2020.
52. Google LLC, "Edge TPU," <https://cloud.google.com/edge-tpu/>.
53. T. Chen, T. Moreau *et al.*, "{TVM}: An Automated {End-to-End} Optimizing Compiler for Deep Learning," in *OSDI*, 2018.
54. D. Shin, J. Lee *et al.*, "DNPU: An 8.1TOPS/W Reconfigurable CNN–RNN Processor for General-Purpose Deep Neural Networks," in *ISSCC*, 2017.
55. Y.-H. Chen, T. Krishna *et al.*, "Eyeriss: An Energy-Efficient Reconfigurable Accelerator for Deep Convolutional Neural Networks," *JSSC*, 2017.
56. Y.-H. Chen, T. Yang *et al.*, "Eyeriss v2: A Flexible Accelerator for Emerging Deep Neural Networks on Mobile Devices," *JETCAS*, 2019.
57. A. Parashar, M. Rhu *et al.*, "SCNN: An Accelerator for Compressed-Sparse Convolutional Neural Networks," in *ISCA*, 2017.
58. S. Han, X. Liu *et al.*, "EIE: Efficient Inference Engine on Compressed Deep Neural Network," in *ISCA*, 2016.
59. D. Kim, T. Na *et al.*, "DeepTrain: A Programmable Embedded Platform for Training Deep Neural Networks," *TCAD*, 2018.
60. M. Gao, X. Yang *et al.*, "TANGRAM: Optimized Coarse-Grained Dataflow for Scalable NN Accelerators," in *ASPLOS*, 2019.
61. S. Han, J. Kang *et al.*, "ESE: Efficient Speech Recognition Engine with Sparse LSTM on FPGA," in *FPGA*, 2017.
62. X. Zhang, X. Liu *et al.*, "High-Performance Video Content Recognition with Long-Term Recurrent Convolutional Network for FPGA," in *FPL*, 2017.
63. M. Gao, J. Pu *et al.*, "TETRIS: Scalable and Efficient Neural Network Acceleration with 3D Memory," in *ASPLOS*, 2017.
64. A. Boroumand, S. Ghose *et al.*, "Google Workloads for Consumer Devices: Mitigating Data Movement Bottlenecks," in *ASPLOS*, 2018.
65. M. Imani, S. Gupta *et al.*, "FloatPIM: In-Memory Acceleration of Deep Neural Network Training with High Precision," in *ISCA*, 2019.
66. S. Koppula, L. Orosa *et al.*, "EDEN: Enabling Energy-Efficient, High-Performance Deep Neural Network Inference Using Approximate DRAM," in *MICRO*, 2019.
67. J. Liu, H. Zhao *et al.*, "Processing-in-Memory for Energy-Efficient Neural Network Training: A Heterogeneous Approach," in *MICRO*, 2018.

68. C. Min, J. Mao *et al.*, "NeuralHMC: An Efficient HMC-Based Accelerator for Deep Neural Networks," in *ASP-DAC*, 2019.
69. S. Cho, H. Choi *et al.*, "McDRAM v2: In-Dynamic Random Access Memory Systolic Array Accelerator to Address the Large Model Problem in Deep Neural Networks on the Edge," *IEEE Access*, 2020.
70. A. Shafiee, A. Nag *et al.*, "ISAAC: A Convolutional Neural Network Accelerator with In-Situ Analog Arithmetic in Crossbars," in *ISCA*, 2016.
71. C. Eckert, X. Wang *et al.*, "Neural Cache: Bit-Serial In-Cache Acceleration of Deep Neural Networks," in *ISCA*, 2018.
72. P. Chi, S. Li *et al.*, "PRIME: A Novel Processing-in-Memory Architecture for Neural Network Computation in ReRAM-Based Main Memory," in *ISCA*, 2016.
73. M. Peemen, A. A. Setio *et al.*, "Memory-Centric Accelerator Design for Convolutional Neural Networks," in *ICCD*, 2013.
74. S. Ghose, A. Boroumand *et al.*, "Processing-in-Memory: A Workload-Driven Perspective," *IBM JRD*, 2019.
75. O. Mutlu, S. Ghose *et al.*, "A Modern Primer on Processing in Memory," in *Emerging Computing: From Devices to Systems — Looking Beyond Moore and Von Neumann*. Springer, 2021.
76. G. F. Oliveira, J. Gómez-Luna *et al.*, "DAMOV: A New Methodology and Benchmark Suite for Evaluating Data Movement Bottlenecks," *IEEE Access*, 2021.
77. S. Ghose, K. Hsieh *et al.*, "The Processing-in-Memory Paradigm: Mechanisms to Enable Adoption," in *Beyond-CMOS Technologies for Next Generation Computer Design*, 2019.
78. O. Mutlu, S. Ghose *et al.*, "Processing Data Where It Makes Sense: Enabling In-Memory Computation," *MicPro*, 2019.
79. O. Mutlu, S. Ghose *et al.*, "Enabling Practical Processing in and Near Memory for Data-Intensive Computing," in *DAC*, 2019.
80. O. Mutlu and L. Subramanian, "Research Problems and Opportunities in Memory Systems," *SUPERFRI*, 2014.
81. O. Mutlu, "Memory Scaling: A Systems Architecture Perspective," in *IMW*, 2013.
82. G. H. Loh, N. Jayasena *et al.*, "A Processing in Memory Taxonomy and a Case for Studying Fixed-Function PIM," in *WoNDP*, 2013.
83. R. Balasubramonian, J. Chang *et al.*, "Near-Data Processing: Insights from a MICRO-46 Workshop," *IEEE Micro*, 2014.
84. H. S. Stone, "A Logic-in-Memory Computer," *IEEE Trans. Comput.*, 1970.
85. A. Saulsbury, F. Pong, and A. Nowatzky, "Missing the Memory Wall: The Case for Processor/Memory Integration," in *ISCA*, 1996.
86. A. Farmahini-Farahani, J. H. Ahn *et al.*, "NDA: Near-DRAM Acceleration Architecture Leveraging Commodity DRAM Devices and Standard Memory Modules," in *HPCA*, 2015.
87. O. O. Babarinsa and S. Idreos, "JAFAR: Near-Data Processing for Databases," in *SIGMOD*, 2015.
88. F. Devaux, "The True Processing in Memory Accelerator," in *Hot Chips*, 2019.
89. N. M. Ghiasi, J. Park *et al.*, "GenStore: A High-Performance and Energy-Efficient In-Storage Computing System for Genome Sequence Analysis," in *ASPLOS*, 2022.
90. J. Gómez-Luna, I. El Hajj *et al.*, "Benchmarking Memory-Centric Computing Systems: Analysis of Real Processing-in-Memory Hardware," in *CUT*, 2021.
91. J. Gómez-Luna, I. E. Hajj *et al.*, "Benchmarking a New Paradigm: An Experimental Analysis of a Real Processing-in-Memory Architecture," arXiv:2105.03814 [cs.AR], 2021.
92. J. Gómez-Luna, I. El Hajj *et al.*, "Benchmarking a New Paradigm: Experimental Analysis and Characterization of a Real Processing-in-Memory System," *IEEE Access*, 2022.
93. C. Giannoula, N. Vijaykumar *et al.*, "SynCron: Efficient Synchronization Support for Near-Data-Processing Architectures," in *HPCA*, 2021.
94. G. Singh, D. Diamantopoulos *et al.*, "NERO: A Near High-Bandwidth Memory Stencil Accelerator for Weather Prediction Modeling," in *FPL*, 2020.
95. S. Lee, K. Kim *et al.*, "A 1ynm 1.25V 8Gb, 16Gb/s/pin GDDR6-based Accelerator-in-Memory Supporting 1TFLOPS MAC Operation and Various Activation Functions for Deep-Learning Applications," in *ISSCC*, 2022.
96. L. Ke, X. Zhang *et al.*, "Near-Memory Processing in Action: Accelerating Personalized Recommendation with AxDIMM," *IEEE Micro*, 2021.
97. C. Giannoula, I. Fernandez *et al.*, "SparseP: Towards Efficient Sparse Matrix Vector Multiplication on Real Processing-in-Memory Architectures," in *SIGMETRICS*, 2022.
98. H. Shin, D. Kim *et al.*, "McDRAM: Low Latency and Energy-Efficient Matrix Computations in DRAM," *IEEE TCADICS*, 2018.
99. A. Denzler, R. Bera *et al.*, "Casper: Accelerating Stencil Computation using Near-Cache Processing," arXiv:2112.14216 [cs.AR], 2021.
100. H. Asghari-Moghaddam, Y. H. Son *et al.*, "Chameleon: Versatile and Practical Near-DRAM Acceleration Ar-

- chitecture for Large Memory Systems,” in *MICRO*, 2016.
101. D. Patterson, T. Anderson *et al.*, “A Case for Intelligent RAM,” *IEEE Micro*, 1997.
  102. D. G. Elliott, M. Stumm *et al.*, “Computational RAM: Implementing Processors in Memory,” *Design and Test of Computers*, vol. 16, Jan. 1999.
  103. M. A. Z. Alves, P. C. Santos *et al.*, “Saving memory movements through vector processing in the dram,” in *Int. Conf. on Compilers, Architecture and Synthesis for Embedded Systems*, 2015.
  104. S. L. Xi, O. Babarinsa *et al.*, “Beyond the wall: Near-data processing for databases,” in *Int. Workshop on Data Management on New Hardware*, 2015.
  105. W. Sun, Z. Li *et al.*, “ABC-DIMM: Alleviating the Bottleneck of Communication in DIMM-Based Near-Memory Processing with Inter-DIMM Broadcast,” in *ISCA*, 2021.
  106. K. K. Matam, G. Koo *et al.*, “GraphSSD: Graph Semantics Aware SSD,” in *ISCA*, 2019.
  107. M. Gokhale, B. Holmes, and K. Iobst, “Processing in Memory: The Terasys Massively Parallel PIM Array,” *Computer*, 1995.
  108. M. Hall, P. Kogge *et al.*, “Mapping Irregular Applications to DIVA, a PIM-Based Data-Intensive Architecture,” in *SC*, 1999.
  109. M. A. Z. Alves, P. C. Santos *et al.*, “Opportunities and Challenges of Performing Vector Operations Inside the DRAM,” in *MEMSYS*, 2015.
  110. E. Lockerman, A. Feldmann *et al.*, “Livia: Data-Centric Computing Throughout the Memory Hierarchy,” in *ASPLOS*, 2020.
  111. J. Ahn, S. Hong *et al.*, “A Scalable Processing-in-Memory Accelerator for Parallel Graph Processing,” in *ISCA*, 2015.
  112. L. Nai, R. Hadidi *et al.*, “GraphPIM: Enabling Instruction-Level PIM Offloading in Graph Computing Frameworks,” in *HPCA*, 2017.
  113. A. Boroumand, S. Ghose *et al.*, “LazyPIM: An Efficient Cache Coherence Mechanism for Processing-in-Memory,” *CAL*, 2017.
  114. D. Zhang, N. Jayasena *et al.*, “TOP-PIM: Throughput-Oriented Programmable Processing in Memory,” in *HPDC*, 2014.
  115. M. Gao and C. Kozyrakis, “HRL: Efficient and Flexible Reconfigurable Logic for Near-Data Processing,” in *HPCA*, 2016.
  116. J. S. Kim, D. S. Cali *et al.*, “GRIM-Filter: Fast Seed Location Filtering in DNA Read Mapping Using Processing-in-Memory Technologies,” *BMC Genomics*, 2018.
  117. M. Drumond, A. Daglis *et al.*, “The Mondrian Data Engine,” in *ISCA*, 2017.
  118. P. C. Santos, G. F. Oliveira *et al.*, “Operand Size Reconfiguration for Big Data Processing in Memory,” in *DATE*, 2017.
  119. G. F. Oliveira, P. C. Santos *et al.*, “NIM: An HMC-Based Machine for Neuron Computation,” in *ARC*, 2017.
  120. J. Ahn, S. Yoo *et al.*, “PIM-Enabled Instructions: A Low-Overhead, Locality-Aware Processing-in-Memory Architecture,” in *ISCA*, 2015.
  121. D. Kim, J. Kung *et al.*, “Neurocube: A Programmable Digital Neuromorphic Architecture with High-Density 3D Memory,” in *ISCA*, 2016.
  122. P. Gu, S. Li *et al.*, “Leveraging 3D Technologies for Hardware Security: Opportunities and Challenges,” in *GLSVLSI*, 2016.
  123. A. Boroumand, S. Ghose *et al.*, “CoNDA: Efficient Cache Coherence Support for Near-Data Accelerators,” in *ISCA*, 2019.
  124. K. Hsieh, E. Ebrahimi *et al.*, “Transparent Offloading and Mapping (TOM) Enabling Programmer-Transparent Near-Data Processing in GPU Systems,” in *ISCA*, 2016.
  125. D. S. Cali, G. S. Kalsi *et al.*, “GenASM: A High-Performance, Low-Power Approximate String Matching Acceleration Framework for Genome Sequence Analysis,” in *MICRO*, 2020.
  126. S. H. Pugsley, J. Jestes *et al.*, “NDC: Analyzing the Impact of 3D-Stacked Memory+Logic Devices on MapReduce Workloads,” in *ISPASS*, 2014.
  127. A. Pattnaik, X. Tang *et al.*, “Scheduling Techniques for GPU Architectures with Processing-in-Memory Capabilities,” in *PACT*, 2016.
  128. B. Akin, F. Franchetti, and J. C. Hoe, “Data Reorganization in Memory Using 3D-Stacked DRAM,” in *ISCA*, 2015.
  129. K. Hsieh, S. Khan *et al.*, “Accelerating Pointer Chasing in 3D-Stacked Memory: Challenges, Mechanisms, Evaluation,” in *ICCD*, 2016.
  130. J. H. Lee, J. Sim, and H. Kim, “BSSync: Processing Near Memory for Machine Learning Workloads with Bounded Staleness Consistency Models,” in *PACT*, 2015.
  131. A. Boroumand, S. Ghose *et al.*, “Mitigating Edge Machine Learning Inference Bottlenecks: An Empirical Study on Accelerating Google Edge Models,” arXiv:2103.00768 [cs.AR], 2021.
  132. A. Boroumand, S. Ghose *et al.*, “Polynesia: Enabling High-Performance and Energy-Efficient Hybrid Transactional/Analytical Databases with Hardware/Software Co-Design,” in *ICDE*, 2022.
  133. A. Boroumand, S. Ghose *et al.*, “Polynesia: Enabling Effective Hybrid Transactional/Analytical Databases with Specialized Hardware/Software Co-Design,” arXiv:2103.00798 [cs.AR], 2021.



134. A. Boroumand, "Practical Mechanisms for Reducing Processor-Memory Data Movement in Modern Workloads," Ph.D. dissertation, Carnegie Mellon University, 2020.
135. M. Besta, R. Kanakagiri *et al.*, "Sisa: Set-centric instruction set architecture for graph mining on processing-in-memory systems," in *MICRO*, 2021.
136. I. Fernandez, R. Quislan *et al.*, "NATSA: A Near-Data Processing Accelerator for Time Series Analysis," in *ICCD*, 2020.
137. G. Singh, G. *et al.*, "NAPEL: Near-Memory Computing Application Performance Prediction via Ensemble Learning," in *DAC*, 2019.
138. Y.-C. Kwon, S. H. Lee *et al.*, "A 20nm 6GB Function-in-Memory DRAM, Based on HBM2 with a 1.2 TFLOPS Programmable Computing Unit using Bank-Level Parallelism, for Machine Learning Applications," in *ISSCC*, 2021.
139. S. Lee, S.-h. Kang *et al.*, "Hardware Architecture and Software Stack for PIM Based on Commercial DRAM Technology: Industrial Product," in *ISCA*, 2021.
140. D. Niu, S. Li *et al.*, "184QPS/W 64Mb/mm<sup>2</sup> 3D Logic-to-DRAM Hybrid Bonding with Process-Near-Memory Engine for Recommendation System," in *ISSCC*, 2022.
141. Q. Zhu, T. Graf *et al.*, "Accelerating Sparse Matrix-Matrix Multiplication with 3D-Stacked Logic-in-Memory Hardware," in *HPEC*, 2013.
142. E. Azarkhish, C. Pfister *et al.*, "Logic-Base Interconnect Design for Near Memory Computing in the Smart Memory Cube," *IEEE VLSI*, 2016.
143. E. Azarkhish, D. Rossi *et al.*, "Neurostream: Scalable and Energy Efficient Deep Learning with Smart Memory Cubes," *TPDS*, 2018.
144. Q. Guo, N. Alachiotis *et al.*, "3D-Stacked Memory-Side Acceleration: Accelerator and System Design," in *WoNDP*, 2014.
145. J. P. C. de Lima, P. C. Santos *et al.*, "Design Space Exploration for PIM Architectures in 3D-Stacked Memories," in *CF*, 2018.
146. B. Akın, J. C. Hoe, and F. Franchetti, "HAMLeT: Hardware Accelerated Memory Layout Transform within 3D-Stacked DRAM," in *HPEC*, 2014.
147. Y. Huang, L. Zheng *et al.*, "A Heterogeneous PIM Hardware-Software Co-Design for Energy-Efficient Graph Processing," in *IPDPS*, 2020.
148. G. Dai, T. Huang *et al.*, "GraphH: A Processing-in-Memory Architecture for Large-Scale Graph Processing," *TCAD*, 2018.
149. P.-A. Tsai, C. Chen, and D. Sanchez, "Adaptive Scheduling for Systems with Asymmetric Memory Hierarchies," in *MICRO*, 2018.
150. P. Gu, X. Xie *et al.*, "iPIM: Programmable In-Memory Image Processing Accelerator using Near-Bank Architecture," in *ISCA*, 2020.
151. A. Farmahini-Farahani, J. H. Ahn *et al.*, "DRAMA: An Architecture for Accelerated Processing Near Memory," *Computer Architecture Letters*, 2014.
152. H. Asghari-Moghaddam, A. Farmahini-Farahani *et al.*, "Near-DRAM Acceleration with Single-ISA Heterogeneous Processing in Standard Memory Modules," *IEEE Micro*, 2016.
153. J. Huang, R. R. Puli *et al.*, "Active-Routing: Compute on the Way for Near-Data Processing," in *HPCA*, 2019.
154. C. D. Kersey, H. Kim, and S. Yalamanchili, "Lightweight SIMT Core Designs for Intelligent 3D Stacked DRAM," in *MEMSYS*, 2017.
155. J. Li, X. Wang *et al.*, "PIMS: A Lightweight Processing-in-Memory Accelerator for Stencil Computations," in *MEMSYS*, 2019.
156. J. S. Kim, D. Senol *et al.*, "GRIM-Filter: Fast Seed Filtering in Read Mapping using Emerging Memory Technologies," arXiv:1708.04329 [q-bio.GN], 2017.
157. A. Boroumand, S. Ghose *et al.*, "LazyPIM: Efficient Support for Cache Coherence in Processing-in-Memory Architectures," arXiv:1706.03162 [cs.AR], 2017.
158. Y. Zhuo, C. Wang *et al.*, "GraphQ: Scalable PIM-Based Graph Processing," in *MICRO*, 2019.
159. M. Zhang, Y. Zhuo *et al.*, "GraphP: Reducing Communication for PIM-Based Graph Processing with Efficient Data Partition," in *HPCA*, 2018.
160. H. Lim and G. Park, "Triple Engine Processor (TEP): A Heterogeneous Near-Memory Processor for Diverse Kernel Operations," *TACO*, 2017.
161. E. Azarkhish, D. Rossi *et al.*, "A Case for Near Memory Computation Inside the Smart Memory Cube," in *EMS*, 2016.
162. M. A. Z. Alves, M. Diener *et al.*, "Large Vector Extensions Inside the HMC," in *DATE*, 2016.
163. J. Jang, J. Heo *et al.*, "Charon: Specialized Near-Memory Processing Architecture for Clearing Dead Objects in Memory," in *MICRO*, 2019.
164. R. Nair, S. F. Antao *et al.*, "Active Memory Cube: A Processing-in-Memory Architecture for Exascale Systems," *IBM JRD*, 2015.
165. R. Hadidi, L. Nai *et al.*, "CAIRO: A Compiler-Assisted Technique for Enabling Instruction-Level Offloading of Processing-in-Memory," *TACO*, 2017.
166. P. C. Santos, G. F. Oliveira *et al.*, "Processing in 3D Memories to Speed Up Operations on Complex Data Structures," in *DATE*, 2018.
167. V. Seshadri, D. Lee *et al.*, "Ambit: In-Memory Accelerator for Bulk Bitwise Operations Using Commodity DRAM Technology," in *MICRO*, 2017.

168. V. Seshadri and O. Mutlu, "In-DRAM Bulk Bitwise Execution Engine," arXiv:1905.09822 [cs.AR], 2019.
169. S. Li, D. Niu *et al.*, "DRISA: A DRAM-Based Reconfigurable In-Situ Accelerator," in *MICRO*, 2017.
170. V. Seshadri, Y. Kim *et al.*, "RowClone: Fast and Energy-Efficient In-DRAM Bulk Data Copy and Initialization," in *MICRO*, 2013.
171. V. Seshadri and O. Mutlu, "The Processing Using Memory Paradigm: In-DRAM Bulk Copy, Initialization, Bitwise AND and OR," arXiv:1610.09603 [cs.AR], 2016.
172. Q. Deng, L. Jiang *et al.*, "DrAcc: A DRAM Based Accelerator for Accurate CNN Inference," in *DAC*, 2018.
173. X. Xin, Y. Zhang, and J. Yang, "ELP2IM: Efficient and Low Power Bitwise Operation Processing in DRAM," in *HPCA*, 2020.
174. L. Song, Y. Zhuo *et al.*, "GraphR: Accelerating Graph Processing Using ReRAM," in *HPCA*, 2018.
175. L. Song, X. Qian *et al.*, "PipeLayer: A Pipelined ReRAM-Based Accelerator for Deep Learning," in *HPCA*, 2017.
176. F. Gao, G. Tziantzioulis, and D. Wentzlaff, "ComputeDRAM: In-Memory Compute Using Off-the-Shelf DRAMs," in *MICRO*, 2019.
177. S. Aga, S. Jeloka *et al.*, "Compute Caches," in *HPCA*, 2017.
178. D. Fujiki, S. Mahlke, and R. Das, "Duality Cache for Data Parallel Acceleration," in *ISCA*, 2019.
179. V. Seshadri, D. Lee *et al.*, "Buddy-RAM: Improving the Performance and Efficiency of Bulk Bitwise Operations Using DRAM," arXiv:1611.09988 [cs.AR], 2016.
180. V. Seshadri and O. Mutlu, "Simple Operations in Memory to Reduce Data Movement," in *Advances in Computers, Volume 106*, 2017.
181. V. Seshadri, Y. Kim *et al.*, "RowClone: Accelerating Data Movement and Initialization Using DRAM," arXiv:1805.03502 [cs.AR], 2018.
182. V. Seshadri, K. Hsieh *et al.*, "Fast Bulk Bitwise AND and OR in DRAM," *CAL*, 2015.
183. S. Li, C. Xu *et al.*, "Pinatubo: A Processing-in-Memory Architecture for Bulk Bitwise Operations in Emerging Non-Volatile Memories," in *DAC*, 2016.
184. J. D. Ferreira, G. Falcao *et al.*, "pLUTo: In-DRAM Lookup Tables to Enable Massively Parallel General-Purpose Computation," arXiv:2104.07699 [cs.AR], 2021.
185. J. D. Ferreira, G. Falcao *et al.*, "pLUTo: Enabling Massively Parallel Computation in DRAM via Lookup Tables," in *MICRO*, 2022.
186. Z. He, L. Yang *et al.*, "Sparse BD-Net: A Multiplication-Less DNN with Sparse Binarized Depth-Wise Separable Convolution," *JETC*, 2020.
187. J. Park, R. Azizi *et al.*, "Flash-Cosmos: In-Flash Bulk Bitwise Operations Using Inherent Computation Capability of NAND Flash Memory," in *MICRO*, 2022.
188. M. S. Truong, L. Shen *et al.*, "Adapting the RACER Architecture to Integrate Improved In-ReRAM Logic Primitives," *JETCAS*, 2022.
189. M. S. Truong, E. Chen *et al.*, "RACER: Bit-Pipelined Processing using Resistive Memory," in *MICRO*, 2021.
190. A. Olgun, M. Patel *et al.*, "QUAC-TRNG: High-Throughput True Random Number Generation Using Quadruple Row Activation in Commodity DRAMs," in *ISCA*, 2021.
191. J. S. Kim, M. Patel *et al.*, "D-RaNGe: Using Commodity DRAM Devices to Generate True Random Numbers With Low Latency and High Throughput," in *HPCA*, 2019.
192. J. S. Kim, M. Patel *et al.*, "The DRAM Latency PUF: Quickly Evaluating Physical Unclonable Functions by Exploiting the Latency-Reliability Tradeoff in Modern Commodity DRAM Devices," in *HPCA*, 2018.
193. F. N. Bostanci, A. Olgun *et al.*, "DR-STRaNGe: End-to-End System Design for DRAM-Based True Random Number Generators," in *HPCA*, 2022.
194. A. Olgun, J. G. Luna *et al.*, "PiDRAM: A Holistic End-to-End FPGA-Based Framework for Processing-in-DRAM," *TACO*, 2022.
195. M. F. Ali, A. Jaiswal, and K. Roy, "In-Memory Low-Cost Bit-Serial Addition Using Commodity DRAM Technology," in *TCAS-I*, 2019.
196. S. Angizi and D. Fan, "GraphiDe: A Graph Processing Accelerator Leveraging In-DRAM-Computing," in *GLSVLSI*, 2019.
197. S. Li, A. O. Glova *et al.*, "SCOPE: A Stochastic Computing Engine for DRAM-Based In-Situ Accelerator," in *MICRO*, 2018.
198. A. Subramaniyan and R. Das, "Parallel Automata Processor," in *ISCA*, 2017.
199. Y. Zha and J. Li, "Hyper-AP: Enhancing Associative Processing Through A Full-Stack Optimization," in *ISCA*, 2020.
200. D. Fujiki, S. Mahlke, and R. Das, "In-Memory Data Parallel Processor," in *ASPLOS*, 2018.
201. L. Orosa, Y. Wang *et al.*, "CODIC: A Low-Cost Substrate for Enabling Custom In-DRAM Functionalities and Optimizations," in *ISCA*, 2021.
202. M. Sharad, D. Fan, and K. Roy, "Ultra Low Power Associative Computing with Spin Neurons and Resistive Crossbar Memory," in *DAC*, 2013.
203. S. H. S. Rezaei, M. Modarressi *et al.*, "NoM: Network-on-Memory for Inter-Bank Data Transfer in Highly-Banked Memories," *CAL*, 2020.
204. UPMEM, "UPMEM Website," <https://www.upmem.com>, 2020.

205. UPMEM, "Introduction to UPMEM PIM. Processing-in-memory (PIM) on DRAM Accelerator (White Paper)," 2018.
206. N. Hajinazar, G. F. Oliveira *et al.*, "SIMDRAM: A Framework for Bit-Serial SIMD Processing Using DRAM," in *ASPLOS*, 2021.
207. S. Williams, A. Waterman, and D. Patterson, "Roofline: An Insightful Visual Performance Model for Multicore Architectures," *CACM*, 2009.
208. J. W. Choi, D. Bedard *et al.*, "A Roofline Model of Energy," in *IPDPS*, 2013.
209. X. Lin, C. Zhao, and W. Pan, "Towards Accurate Binary Convolutional Neural Network," in *NIPS*, 2017.
210. X. Xiang, Y. Qian, and K. Yu, "Binary Deep Neural Networks for Speech Recognition," in *INTERSPEECH*, 2017.
211. H. Qin, Z. Cai *et al.*, "BiPointNet: Binary Neural Network for Point Clouds," *arXiv:2010.05501 [cs.CV]*, 2020.
212. T. Chen, Z. Zhang *et al.*, "BNN-BN=?": Training Binary Neural Networks Without Batch Normalization," in *CVPR*, 2021.
213. NVIDIA, "NVIDIA A100 Tensor Core GPU Architecture. White Paper," <https://images.nvidia.com/aem-dam/en-zz/Solutions/data-center/nvidia-ampere-architecture-whitepaper.pdf>, 2020.
214. J. Choquette and W. Gandhi, "NVIDIA A100 GPU: Performance & Innovation for GPU Computing," in *Hot Chips*, 2020.
215. NVIDIA, "CUDA Basic Linear Algebra Subroutine (cuBLAS) Library," <https://docs.nvidia.com/cuda/cublas/index.html>, 2022.
216. JEDEC Solid State Technology Assn., "JESD23-5D: High Bandwidth Memory (HBM) DRAM Standard," March 2021.
217. Y.-B. Kim and T. W. Chen, "Assessing Merged DRAM/Logic Technology," in *ISCA*, 1996.
218. C. Li, R. Ausavarungnirun *et al.*, "A Framework for Memory Oversubscription Management in Graphics Processing Units," in *ASPLOS*, 2019.
219. R. Ausavarungnirun, J. Landgraf *et al.*, "Mosaic: A GPU Memory Manager with Application-Transparent Support for Multiple Page Sizes," in *MICRO*, 2017.
220. R. Ausavarungnirun, V. Miller *et al.*, "MASK: Redesigning the GPU Memory Hierarchy to Support Multi-Application Concurrency," in *ASPLOS*, 2018.
221. D. U. Lee, K. W. Kim *et al.*, "A 1.2V 8Gb 8-Channel 128GB/s High-Bandwidth Memory (HBM) Stacked DRAM with Effective Microbump I/O Test Methods Using 29nm Process and TSV," in *ISSCC*, 2014.
222. Hybrid Memory Cube Consortium, "Hybrid Memory Cube Specification Rev. 2.0," <http://www.hybridmemorycube.org/>.
223. D. Lee, S. Ghose *et al.*, "Simultaneous Multi-Layer Access: Improving 3D-Stacked Memory Bandwidth at Low Cost," *TACO*, 2016.
224. H. Kwon, P. Chatarasi *et al.*, "Understanding Reuse, Performance, and Hardware Cost of DNN Dataflow: A Data-Centric Approach," in *MICRO*, 2019.
225. M. Poletto and V. Sarkar, "Linear Scan Register Allocation," *TOPLAS*, 1999.
226. I. Goodfellow, Y. Bengio, and A. Courville, *Deep Learning*. MIT Press, 2016.
227. K. K. Chang, P. J. Nair *et al.*, "Low-Cost Inter-Linked Subarrays (LISA): Enabling Fast Inter-Subarray Data Movement in DRAM," in *HPCA*, 2016.
228. A. Krizhevsky, "Convolutional Deep Belief Networks on CIFAR-10," <https://www.cs.toronto.edu/~kriz/conv-cifar10-aug2010.pdf>, 2010.
229. L. Deng, "The MNIST Database of Handwritten Digit Images for Machine Learning Research [Best of the Web]," *IEEE Signal Processing Magazine*, 2012.
230. G. M. Amdahl, "Validity of the Single Processor Approach to Achieving Large Scale Computing Capabilities," in *AFIPS*, 1967.
231. N. Binkert, B. Beckmann *et al.*, "The gem5 Simulator," *Comput. Archit. News*, 2011.
232. Intel Corp., "6th Generation Intel Core Processor Family Datasheet," <http://www.intel.com/content/www/us/en/processors/core/>.
233. NVIDIA Corp., "NVIDIA Titan V," <https://www.nvidia.com/en-us/titan/titan-v/>.

**Geraldo F. Oliveira** is currently with ETH Zürich, Zürich, Switzerland. Contact him at geraldod@safari.ethz.ch.

**Juan Gómez-Luna** is currently with ETH Zürich, Zürich, Switzerland. He is a Member of IEEE. Contact him at juan.gomez@safari.ethz.ch.

**Saugata Ghose** is currently with the University of Illinois Urbana-Champaign, Urbana, IL, USA. He is a Member of IEEE. Contact him at ghose@illinois.edu.

**Amirali Boroumand** is currently with Google, Mountain View, CA, USA. Contact him at amirali.boroumand@gmail.com.

**Onur Mutlu** is currently with ETH Zürich, Zürich, Switzerland and Carnegie Mellon University, Pittsburgh, PA, USA. He is a Fellow of IEEE. Contact him at omutlu@gmail.com.